International Journal of Modern Manufacturing Technologies
ISSN 2067–3604, Vol. VII, No. 1 / 2015

SUPERELASTIC-LIKE RESPONSE OBTAINED AT Fe-Mn-Si-C_r SHAPE MEMORY ALLOYS PROCESSED BY HIGH-SPEED HIGH PRESSURE TORSION

Gheorghe Gurău[1], Leandru G. Bujoreanu[2], Carmela Gurău[2], Radu I. Comăneci[2], Nicoleta M. Lohan[2], Bogdan Pricop[2], Marius G. Suru[2]

[1] "Dunărea de Jos" University of Galați Faculty of Engineering
Str. Domnească 111, 800201 Galați, Romania
[2]"Gheorghe Asachi" Technical University of Iasi, Faculty of Material Science and Engineering
Bd. D. Mangeron 61A, 700050, Iasi, Romania

Corresponding author: Leandru Bujoreanu, lgbujor@tuiasi.ro

Abstract: By means of an original high speed high pressure torsion procedure, coned-disk spring shape modules, with hardness gradient along their generators, were produced from an Fe-28Mn-6Si-7Cr (mass %) shape memory alloy. The modules were subjected to loading-unloading compression tests by means of deformation devices with three configurations. When compressed between two flat surfaces the modules, with various shape characteristic ratios, developed a superelastic-like response, characterized by force plateaus both on their loading and unloading portions, which preserved their aspect and were reproducible during isothermal cycling, at different temperatures between room temperature and 473 K. The presence of force plateaus was confirmed by lubricated compression of deformed (flat) modules. Maintaining the prescribed level of compression force has the potential to contribute to the development of axial-displacement compensation devices, such as those necessary for wear compensation at radial-axial bearings.
Key words: Shape memory alloys; phase transformation; severe plastic deformation; high speed high pressure torsion; mechanical testing; optical microscopy.

1. INTRODUCTION

Fe-Mn-Si – based shape memory alloys (SMAs) have been intensely studied in the past three decades due to the cumulation of several beneficial economical (low cost) [1] mechanical (high recovery stress) [2] and technological (high plasticity, workability and weldability) properties, which recommend these SMAs as potential low-cost replacers of Ti-Ni based ones. This endeavor enabled the development of Fe-Mn-Si – based SMAs under two commercial forms: Fe-28 Mn-6 Si-5 Cr [3] and Fe-14 Mn-5 Si-9 Cr-5 Ni (mass. %, as all compositions will be listed hereinafter), which have been successfully used for constrained recovery [4] applications, such as pipe couplings, fishplates for crane rail fastening and concrete pre-straining rods [6].

On the other hand, it is well known that, unlike shape memory effect (SME), which is characteristic to all SM materials, superelasticity (SE) is present only in some SMAs. Superelasticity (SE) is associated with the presence of at least one force (stress) plateau both on loading and unloading portions of the force (stress)-displacement (strain) isothermal curves that, under certain conditions, enable the material to fully recover its original shape, after one loading-unloading cycle [5]. From structural point of view, SE is the effect of a reversible stress-induced martensitic transformation, such as those identified in Ti-Ni, Cu-Al-Ni, Cu-Zn-Al and Fe-Ni-Co [7] based SMAs. In the case of Fe-Mn-Si – based SMAs, it was argued that no SE can occur, due to the non-thermoelastic character of γ (face center cubic, fcc) → ε (hexagonal close-packed, hcp) stress-induced martensitic transformation which causes irreversible slip during the deformation above critical temperatures of reverse martensitic transformation [8].
The present work aims to report the superelastic-like response of Fe-Mn-Si – based specimens with special configuration, when subjected to static compression loading-unloading, between flat surfaces.

2. MATERIAL AND METHODS

Fe-28Mn-6Si-5Cr SMA ingots were obtained through cold crucible induction melting from high purity elemental powders (over 99%), using a Fives Celes furnace. By spark erosion, tensile specimens were cut experiencing static failure at ultimate stress and strain of approximately 644MPa and 27 %, respectively. Further hot rolling and new spark erosion cutting enabled to obtain new specimens with marked augmentation of tensile failure parameters which reached approx. 950MPa and 54%, respectively. Both

as cast and hot worked specimens, after room temperature pre-straining, experienced the formation of stress-induced martensite, as revealed by optical microcopy, on the polished surface of pre-strained tensile specimens cut from ingots.

During heating, the thermally induced reversion of martensite to austenite was accompanied by SME. The start and finish temperatures of reverse martensitic transformation were evaluated by differential scanning calorimetry (DSC), on fragments cut from undeformed specimens (A_s=117^{0}C and A_f=161^{0}C) and by cinematographic analysis [9] of films recorded during heating-induced free recovery of initial shape of hot rolled specimens, bent at room temperature (A_s = 137^{0}C and A_f = 316^{0}C).

The ingots were machined and axially-drilled, before cutting circular crowns with dimensions Φ (18-8)×2 mm. Each individual circular crown was further processed by high speed-high pressure torsion (HS-HPT) according to an original procedure [10] and coned-disk spring shape modules were obtained. By accurate pressure adjustment, high pressure torsioned (HPT'd) modules with different height and wall thickness were produced. Throughout details, concerning HS-HPT technology have been recently provided, [11]. These modules were machined, so as to adjust and to render parallel upper and lower surfaces. Further, the modules were tested in static compression with a deformation rate of 0.5 mm/ min, by means of an INSTRON 3382 testing machine with thermal chamber. As schematized in Fig.1, the tests were applied, without any lubrication on active surfaces, by means of three types of deformation devices with: (i) with flat surfaces, Fig.1(a); (ii) with centered taper reversion, Fig.1(b) and (iii) with centered flat surfaces, Fig.1(c). Besides device configuration, Fig.1 also illustrates the specimen geometry and expected deformation during compression loading mode according to finite element modeling (FEM), of HPT'd coned-disk spring shape modules.

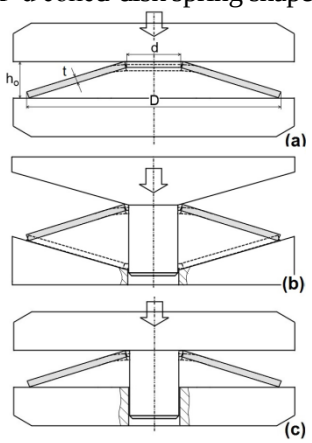

Fig. 1. Schematic illustration of compression loading mode and expected deformation by FEM modeling of HPT'd coned-disk spring shape modules between three types of deformation devices with: (a) flat surfaces; (b) centered taper reversing and (c) centered flat surfaces.

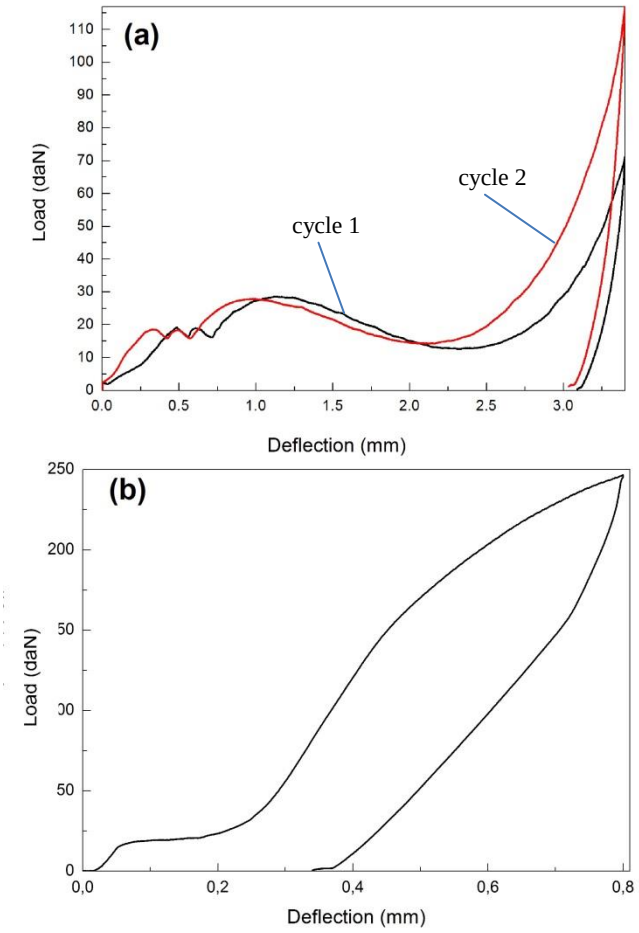

Fig. 2. Load-deflection curves obtained by means of deformation devices with: (a) centered taper reversing and (b) centered flat surfaces

It is assumed that the initial deformation (bending) of smaller (inner) diameter area, predicted by FEM, was caused by the hardness gradient developed by HPT along module's generators. During HPT processing, the circular crown billet turned into a truncated cone shell, by maintaining its inner diameter almost constant, while severe plastic deformation caused thickness decrease, up to 75 % accompanied by outer diameter increasing up to 55 %. As an effect of non-uniform severe deformation, the average hardness values measured along cone generator (under 50 g load applied for 25 s), gradually increased from an average of 322HV50/25, in the area of inner diameter, to a mean value of 366HV50/25, in the area of outer diameter.

Structural analysis was performed on three modules with different states: (i) initial, after HPT; (ii) compressed, after one loading-unloading cycle applied between flat surface devices and (iii) after one additional unconstrained heating, up to 1800C.

The three modules were diametrically cut with low rate saw and embedded into cold mounting resin, before being metallographically prepared by grinding up to 2400 mesh, polishing with 0.04 μm alumina powder and etching with a solution of 1.2% K2S2O5

+ 1% NH4HF2 in 100 ml distilled water. The specimens were structurally analyzed by X-ray diffraction (XRD) as well as optical (OM) and scanning electron (SEM) microcopy, performed on a BRUKER AXS D8 Advance diffractometer with Cu Kα, an OPTIKA XDS-3 MET microscope equipped with OPTIKAM 4083.B5 microscopy digital USB camera operated with OPTIKAM B5 software and a FEI Quanta SEM 200 3D dual beam microscope, respectively.

3. RESULTS AND DISCUSSIONS

Coned-disk springs can be described by the shape characteristic ratio, obtained by dividing free height (H0-t, maximum possible deflection) to spring thickness (t), [12]. Different modules with different shape characteristic ratios were subjected to compression loading-unloading cycles applied, without lubrication, by means of the three deformation devices, shown in Fig. 3. The recorded load-deflection curves displayed different characteristics for each of the three devices. For example, Fig. 2 shows the load deflection curves obtained by means of deformation devices with centered taper reversing, Fig. 2(a) and h centered flat surfaces, Fig. 2(b).

The present discussion is focused on the results obtained during compression loading-unloading cycles applied by means of the flat surface devices shown in Fig. 1(a), without lubrication.

Figure 3 illustrates the load-deflection responses recorded during one compression cycle applied with flat-surface devices, to three modules with different shape characteristic ratios, namely 0.9, 1.3 and 2.8, respectively.

Load plateaus can be observed on both loading and unloading portions of the curves, of each of the three tested modules. Total deflection was 1 mm/ cycle while the length of loading and unloading plateaus ranged between 0.4 and 0.43mm.

Unlike other superelastic SMAs, in the case of present HPT'd modules, force plateaus cannot be exclusively associated with a reversible stress-induced martensitic transformation but more likely to the presence of hardness gradient which enables the gradual migration of bent section, along cone's generator, from inner to outer diameter area. This particular behavior differentiates HPT'd modules from common disk springs, where Young's modulus is assumed linear and spring flank remains rectangular by rotating around a center of rotation during deflection [13]. The presence of force plateaus was confirmed, for the module with 0.9 shape characteristic ratio, being reproducible for as much as 13 cycles, as shown in Fig. 4. The number of cycles was limited due to the accumulation of successive plastic deformations which finally rendered the module completely flat and further force increase occurred in an exponential manner. It should be noted that the force plateaus have been reproducible even when the modules were tested to dry compression between flat surfaces at elevated temperatures, as high as 2000C.

Completely deformed (flat) modules were further subjected to compression experiments performed between lubricated flat surfaces. Force plateaus were observed only in initial deformation stage, in this case, and force increased to much higher values. The formation of ε (hcp) martensite is nevertheless expected to take place after HPT. In addition, when deflection increases beyond the end of loading plateau, stress-induced martensite would also accompany the occurrence of plastic deformation. In spite of plastic deformation, a certain recovery of initial configuration can be expected after unloading, if a mechanism of reversible transformation-induced plasticity, which was previously reported in Fe-Mn-Si SMAs [14] is taken into consideration.

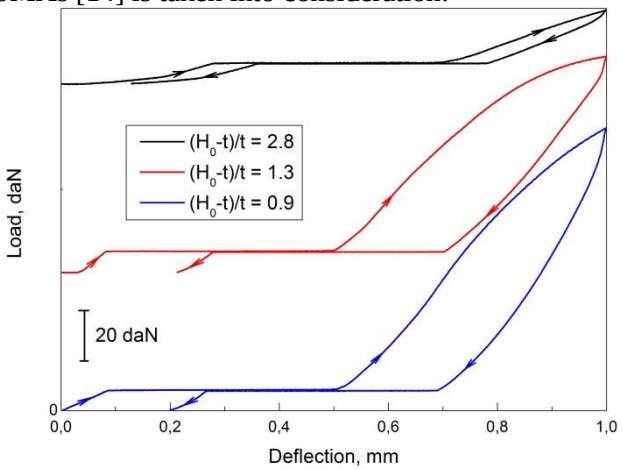

Fig.3. Superelastic-like responses at compression, between flat surfaces, without lubrication, of HPT'd coned-disk spring shape modules with three different shape characteristic ratios.

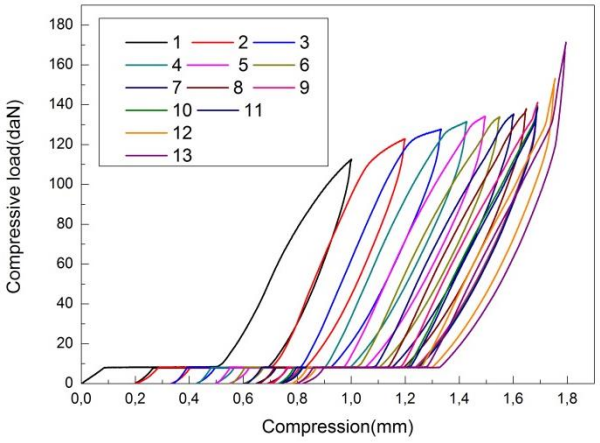

Fig. 4. Reproduction of superelastic-like response of the module with shape characteristic ratio of 0.9, obtained by means of deformation devices with flat surfaces, during 13 cycles

In order to ascertain the presence of ε (hcp) martensite, the three HPT'd modules, in initial, compressed and heated states, respectively, were studied by X-ray diffraction and the results are shown in Fig. 5a.

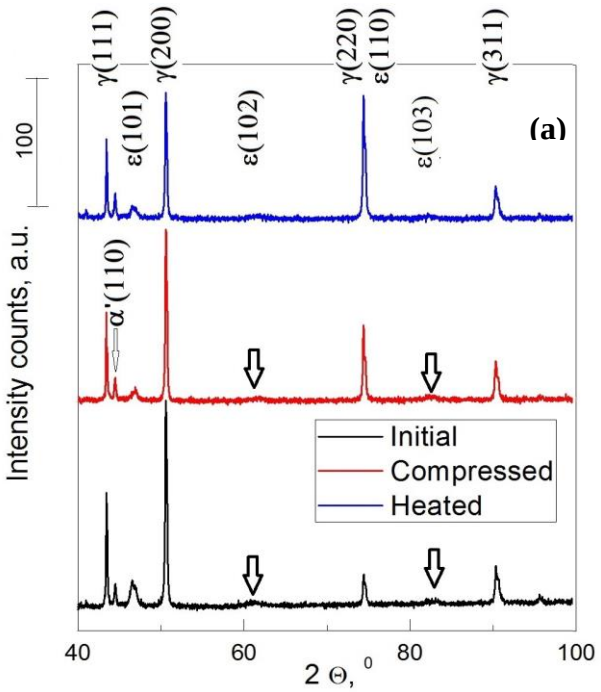

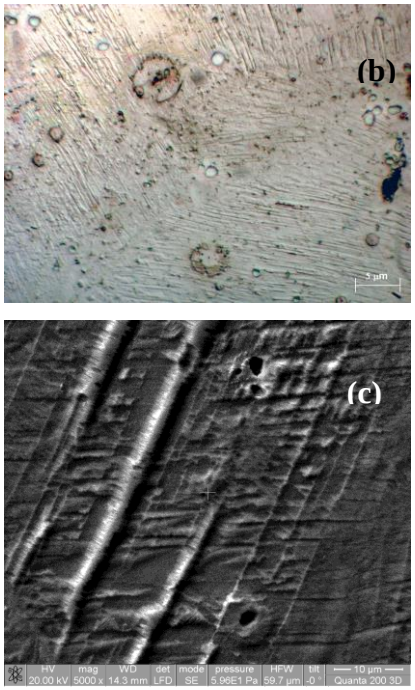

Fig. 5. Typical XRD patterns recorded on three HPT'd modules in initial, compressed and heated states, respectively (a); OM micrograph characteristic to a deformed HPT'd module, illustrating parallel arrays of martensites plates (b);SEM micrograph of a deformed and heated HPT'd module with large α' (bcc) martensite needles (c)

It is obvious that ε (hcp) martensite has been present in the structure of all modules. Semi-quantitative analysis, performed by evaluating the ratios determined by the relative intensities of non-overlapping diffraction maxima γ(111), α'(110), ε(101), γ(200) and γ(311), [15] revealed that the relative amount of ε (hcp) martensite was approx. 5.7 % in initial state, decreased after compression to about 4 % and slightly increased after heating to 4.2 %. On the other hand, α' (body center cubic, bcc) martensite continuously increased from about 5.1% to 6.9 % and finally to 8.8 %, respectively. This could be associated with the large amount of deformation which favors the transformation of ε (hcp) into α' (bcc) martensite [16]. Besides ε(101) martensite plate variant, which has a rather deformed peak, mostly in initial state, the positions of ε(102) and ε(103) variants are indicated in Fig.5a. These broader XRD peaks are indicative of the existence of either small ε (hcp) martensite crystallite size along the direction normal to the specified planes, or distortion (microstrains) of the crystal structure.

In compressed state the presence of martensite was identified on optical micrographs. Figure 5b is an optical micrograph illustrating arrays of parallel martensite plates caused by common orientation of the dislocations, during severe plastic deformation, which was also observed at NiTi SMAs [17]. After heating, an amount of almost 9 % α' (bcc) is expected to exist, this phase being identified as long α' (bcc) martensite needles on the SEM micrograph of Fig.5c. Further, an HPT'd module with 2.8 shape ratio was subjected to a loading-unloading cycle, compressed again, until reaching the end of loading plateau and then heated in the thermal chamber of testing machine, while being in compressed state. This experiment aimed to reveal the presence of constrained recovery SME, illustrated by an increase of recovery force [18]. Considering that dimensional changes accompany thermally induced reversion to γ (fcc) austenite of ε (hcp) stress-induced martensite, even when the latter exists in small amounts [19], it can be assumed that load increase during heating in deformed state, was caused by the reverse martensitic transformation. Critical temperatures of martensite reversion were empirically determined as A_s'= 37^0C and A_f'=134^0C.

4. CONCLUSIONS

A superelastic-like response was obtained during compression loading-unloading cycles, applied between flat surfaces, without using any lubricant, to coned-disk spring shape modules obtained by means of a modified high pressure torsion procedure. This procedure caused the occurrence of a hardness gradient along modules generator, which enabled the gradual elastic bending of truncated shells, from inner to outer diameter areas. This phenomenon seems to be present not only in the modules with truncated cone shells processed by high speed-high

pressure torsion from SMAs but also from other metallic alloys, such as austenitic stainless steel (304). But SMA HPT'd modules have the benefit of developing recovery forces and of recovering initial shape by free recovery heating. The presence of ε (hcp) stress-induced martensite was confirmed by XRD patterns, OM and SEM micrographs, as well as by the development of a recovery force during heating of compressed modules in constrained state. Similar aspects of the superelastic-like response were observed on modules with different shape characteristic ratios, with increasing the number and the temperature of isothermal cycles. The confirmation of force plateaus existence, by lubricated compression of deformed (flat) modules eliminates any doubt regarding the artificial formation of these plateaus. Moreover, maintaining the compression force at a prescribed level, while deflection varies on a given dimensional range, has the potential to contribute to the development of axial-displacement compensation devices, such as those necessary for wear compensation at radial-axial bearings. Further research is necessary to elucidate the mechanism which governs this superelastic-like response.

Acknowledgements
This work was supported by UEFISCDI, through the research project code PN-II-PT-PCCA-2011-3.1-0174, contract no. 144/ 2.07.2012.

5. REFERENCES

1. James, R.D., Hane, K.F., (2000). *Martensitic transformations and shape-memory materials*, Acta Mater., 48, 197-222.
2. Murakami, M., Otsuka, H., Suzuki, H.G., Matsuda, S., (1986). *Complete shape memory effect in polycrystalline Fe-Mn-Si alloys*, in: Proc International Conference on Martensitic Transformation, Japan Institute of Metals, 985–990.
3. Otsuka, H., Yamada, H., Maruyama, T., Tanahashi, H., Matsuda, S., Murakami, M., (1990). *Effects of alloying additions on Fe-Mn-Si shape memory alloys.* ISIJ Int. 30, 674-679.
4. Proft, J.L., Duerig, T.W., (1990). *The mechanical aspects of constraint recovery*, in: Duerig, T.W., Melton, K.N., Stöckel, D., Wayman, C.M. (Eds.) Engineering Aspects of Shape Memory Alloys, Butterworth-Heinemann, London, 115–129.
5. Ma, J., Karaman, I., (2010). *Expanding the repertoire of shape memory alloys*, Science 327, 1468-1469.
6. Lee, W.J., Weber, B., Feltrin, G., Czaderski, C., Motavalli, M., Leinenbach, C., (2013). *Stress recovery behaviour of an Fe–Mn–Si–Cr–Ni–VC shape memory alloy used for prestressing*, Smart Mater Struct 22, 125037.
7. Tanaka, Y., Himuro, Y., Kainuma, R., Sutou, Y., Omori, T., Ishida, K., (2010). *Ferrous polycrystalline shape-memory alloy showing huge superelasticity*, Science 327, 1488-1490.
8. Sawaguchi, T., Kikuchi, T., Kajiwara, S., (2005). *The pseudoelastic behavior of Fe–Mn–Si-based shape memory alloys containing Nb and C*, Smart Mater. Struct., 14, S317-S322.
9. Pricop, B., Söyler, U., Özkal, B., Lohan, N.M., Paraschiv, A.L., Suru, M.G., Bujoreanu, L.-G., (2013). *Influence of mechanical alloying on the behavior of Fe-Mn-Si-Cr-Ni shape memory alloys made by powder metallurgy*, Mater. Sci. Forum 738-739, 237-241.
10. Mahesh, K.K., Braz Fernandes, F.M., Gurău, G., (2012). *Stability of thermal-induced phase transformations in the severely deformed equiatomic Ni–Ti alloys*, J. Mater. Sci. 47, 6005-6014.
11. Gurau, G., Gurau. C., Potecasu, O., Alexandru, P., Bujoreanu, L. G., (2014). *Novel High-Speed High Pressure Torsion Technology for Obtaining Fe-Mn-Si-Cr Shape Memory Alloy Active Elements*, J. Mater. Eng. Perform, DOI: 10.1007/s11665-014-1060-2
12. Ozaki, S., Tsuda, K., Tominaga, J., (2012). *Analyses of static and dynamic behavior of coned disk springs: Effects of friction boundaries*, Thin-Walled Struct., 59, 132-143.
13. http://www.schnorr.com/, Handbook for Springs, Schnorr.
14. Sawaguchi, T., Bujoreanu, L.G., Kikuchi, T., Ogawa, K., Koyama, M., Murakami, M., (2008). *Mechanism of reversible transformation-induced plasticity of Fe–Mn–Si shape memory alloys*, Scripta Mater., 59, 826-829.
15. Sawaguchi, T., Bujoreanu, L.G., Kikuchi, T., Ogawa, K., Yin, F., (2008). *Effects of Nb and C in Solution and in NbC Form on the Transformation-related Internal Friction of Fe–17Mn (mass %) Alloys*, ISIJ Int. 48(1), 99–106.
16. Peng, H., Wen, Y., Liu, G., Wang, C., Li, N., (2011). *A role of α' martensite introduced by thermo-mechanical treatment in improving shape memory effect of an Fe-Mn-Si-Cr-Ni Alloy*, Adv. Eng. Mater. 13, 388-394.
17. Zhang, Y., Jiang, S., Hub, L., Liang, Y., (2013). *Deformation mechanism of NiTi shape memory alloy subjected to severe plastic deformation at low temperature*, Mat. Sci. Eng. A 559, 607–614.
18. Bujoreanu, L.G., Dia, V., Stanciu, S., Susan, M., Baciu, C., (2008). *Study of the tensile constrained recovery behavior of a Fe-Mn-Si shape memory alloy*, Eur. Phys. J. Special Topics, 158, 15-20.
19. Bujoreanu, L.G., Stanciu, S., Comaneci, R.I., Meyer, M., Dia, V., Lohan, C., (2009). *Factors influencing the reversion of stress-induced martensite to austenite in a Fe-Mn-Si-Cr-Ni shape memory alloy*, J. Mater. Eng. Perform., 18, 500-505.

Received: January 14, 2015 / Accepted: June 15, 2015 / Paper available online: June 20, 2015